Effect of Sulfur-Containing Dopants on Filling Efficiency for Conducting Polymers

An Undergraduate Honors Thesis

Victoria Yee

Spring 2018

Presented in Partial Fulfillment of the Requirements for Graduation with Distinction in the Department of Mechanical Engineering at The Ohio State University

Honors Thesis Defense Committee:

Dr. Vishnu Sundaresan – Advisor

Dr. Noriko Katsube

Abstract

Cellular physiology is sensitive to minute changes in the chemical composition of its environment. Therefore, understanding the effect of ionic concentration is significant to understanding healthcare (diagnosis and treatment). Electrically conductive polymers, such as polypyrrole, exchange ions with solution by the application of electrical potentials and thus alter the chemical composition of the solution without the use of microfluidics. Calculation of morphology-dependent parameters, such as filling efficiency, assists in quantifying these transport phenomena. In an effort to understand how conducting polymers may influence cellular physiology, a conducting polymer's cation storage capacity was measured to calculate the ability of the conducting polymer to change the chemical makeup of an ionic solution. Polypyrrole samples were fabricated using three dopants (p-toluene sulfonate, dodecyl sulfate, and dodecylbenzenesulfonate) at charge densities of 0.4 C/cm^2, 0.8 C/cm^2, and 1.2 C/cm^2. These membranes were pretreated with cyclic voltammetry until all ion exchange was reversible and then characterized by chronoamperometry. All tests were conducted with 100 mM potassium chloride solution. The number of ions exchanged by polypyrrole with the solution was calculated by fitting the data to an exponential function used to describe ion transport and compared to the theoretical maximum ion storage of the polypyrrole film. Preliminary findings indicated that filling efficiency (ionic ingress divided by the theoretic maximum) was approximately equal across all dopants. As all three dopants possess a similar morphology, they form polymers with a comparable number of redox sites, and filling efficiency is largely dependent on the number of available redox sites. These findings establish that the filling efficiency of polypyrrole is independent of the dopant for a given dopant morphology.

Acknowledgements

I would foremost like to express my gratitude to Dr. Vishnu Sundaresan for the opportunity to work on this project and the experience I have gained from it. His support and encouragement these last two years have been immense. Additionally, I would like to thank Dr. Noriko Katsube for serving as a member of my defense committee.

This project would also not have been possible without Dr. Robert Northcutt, whose mentorship during my time as a research assistant has been invaluable. I am grateful as well for the assistance and kindness offered to me by everyone at the Integrated Material Systems Lab.

Special thanks go to the National Science Foundation (Award #1512405) for funding this project and The Ohio State University College of Engineering for awarding me an Undergraduate Research Scholarship.

Table of Contents

List of Figures

List of Tables

Chapter 1: Introduction

1.1 Potential Impact of Lab-on-a-Chips on Global Healthcare

Developing countries and geographically remote regions often have limited healthcare resources and infrastructure coupled with inadequate access to clean water and sanitation. Residents of these areas therefore carry a disproportionately heavy burden of disease, with the greatest disparity observed for infectious diseases. For instance, in 2015, 90 percent of reported malaria cases (191 million cases) occurred in Africa. Malaria cases have been declining globally (22 percent drop between 2000 and 2015), but this remains a staggering number of cases [1]. Understandably, the health community in developing countries remains focused on the diagnosis, treatment, and prevention of infectious disease.

However, as developing countries continue to industrialize and rates of infectious diseases decline, attention is expected to transition to non-communicable diseases such as cardiovascular disease and cancer [2]. The burden of disease for non-communicable diseases is equivalent for developing and developed countries, and non-communicable diseases already represent a larger percentage of the total disability-adjusted life years (DALY) than infectious diseases [2], [3]. The following table, Table 1, presents the global DALYs and percentage of total DALY for certain communicable and non-communicable diseases [3]. A more comprehensive list can be found in [3].

Table 1: Global all-age DALYs for years 2005 and 2015 for selected communicable and non-communicable diseases. All values represent median values [3].

	All-age DALYs (thousands)		Percent of Total DALY (%)		Percent Change (%)
	2005	2015	2005	2015	
All Causes	**2,553,306.8**	**2,464,895.4**	**100**	**100**	**-3.50**
Communicable, maternal, neonatal, and nutritional diseases	**968,014.5**	**741,595.9**	**37.9**	**30.1**	**-23.4**
HIV/AIDS	98,916.1	66,689.5	3.87	2.71	-32.6
Tuberculosis	49,769.6	40,302.2	1.95	1.64	-19.0
Malaria	90,438.1	55,769.6	3.54	2.26	-38.3
Diarrhea, lower respiratory, and other common infectious diseases	333,534.0	242,875.8	13.1	9.85	-27.2
Non-communicable diseases	**1,322,207.9**	**1,473,508.2**	**51.8**	**59.8**	**11.4**
Neoplasms	187,562.1	209,359.2	7.35	8.49	11.6
Cardiovascular disease	326,252.4	347,528.9	12.8	14.1	6.50
Diabetes mellitus	122,917.1	146,780.6	4.81	5.95	19.4

Approaches to improving healthcare must be multi-faceted, if the needs of developing countries are to be met. According to a survey conducted by Daar *et. al.*, the three most impactful biotechnologies in developing countries are "modified molecular technologies for affordable, simple diagnosis of infectious diseases [4]"; "recombinant technologies to develop vaccines against infectious diseases [4]"; and "technologies for more efficient drug and vaccine delivery systems [4]". Therefore, emerging technologies should focus on both healthcare diagnosis and treatment while considering the constraints of designing for developing countries. A device designed for the most restrictive settings must be affordable, functional without access to external resources such as electricity or trained medical personnel, operational at a wide range of temperatures, and robust enough to survive rough transport and handling [3].

Lab-on-a-chips (LOCs), devices that scale down one or more laboratory processes onto a microprocessor chip, could revolutionize global healthcare. Benefits offered by LOCs include

mass production potential, minute sample and reagent sizes, portability, multiplexing, and quick response times [2], [5]. LOCs have almost limitless application potential in the healthcare industry, including use as diagnostic equipment, drug delivery systems, environmental monitors, and platforms for cellular testing for biomedical and pharmaceutical research. This functional diversity along with the previously mentioned benefits makes LOCs an ideal technology for use in developing countries and remote settings [2].

Remote settings offer the greatest challenge to those developing LOCs. While the continued construction of centralized testing facilities would sufficiently service many people in developing countries, remote populations will likely always remain dependent on point-of-care devices. These devices would be particularly constrained by cost due to the difficulty and expense of transport, and the overall cost of a single device needs to be on the order of pennies [2]. Despite these constraints, numerous LOCs have been developed to facilitate point-of-care testing [6], [7]. Many more examples of LOCs focused on healthcare are available in [2].

1.1.1 Limitations of Microfluidics

Microfluidics, the control and manipulation of fluids on a scale of typically less than a millimeter, is central to the functionality of many LOCs. At this scale, fluid flow maintains unique properties: flow is almost always laminar; diffusion occurs rapidly; surface-area-to-volume ratios are high; and surface tension forces are significant [8].

Several driving forces exist that can be used to control flow, including pressure gradients and electro-osmosis. Pressure gradients as a control method face two major limitations: difficulty in multidirectional flow control and magnitude of the initial pressure needed to drive flow. Flow in a microchannel using pressure gradients is unidirectional, unless valves are employed. Valves can be used to change the flow direction, but they often leak [5]. According to the Hagen-Poiseuille

equation (Equation 1), the pressure difference between two ends of a channel is inversely proportional to fourth power of the diameter of the channel. In the case of microchannels, the expected pressure differential will be large, and supplying that pressure may be difficult in resource-scarce areas or even harmful to biological samples.

$$\Delta P = \frac{128 \mu L \dot{V}}{\pi D^4} \quad (1)$$

For Equation 1, ΔP represents pressure drop between the two ends of a channel, μ represents dynamic viscosity, L represents length of the channel, $\dot{V}$ represents volumetric flow rate, and D represents diameter of the channel.

Electro-osmosis also has its own share of drawbacks. When multiple channels are interconnected, electroosmotic pumping tends to draw fluid out of the adjoining channels. This undesirable phenomenon can be difficult to control without precise channel design, impedance modeling, and multiple instances of active voltage control [5]. Another limitation is electro-osmosis's incompatibility with certain molecules. Macromolecules, such as proteins, and high-ionic-strength buffers adsorb to channel walls, decreasing electroosmotic pumping efficiency [5], [8].

Further discussion of microfluidic systems, including their strengths and limitations, can be found in [9]. Regardless of the driving force, microfluidic-based LOCs remain dependent on a complicated network of microchannels to function. Coordinating multiple fluids and their interactions becomes difficult.

1.2 Conducting Polymers as an Alternative to Microfluidics

Conducting polymers (CPs) are a unique polymer class that exhibit intrinsic electrical conductivity. When undoped, CPs are electrically insulative, but due to the presence of conjugated

pi double bonds in their backbone, they can exhibit conductivities and other electronic properties on an order similar to that of metals. The novel characteristics of CPs have therefore allowed them to permeate into a multitude of fields in versatile applications from fuel cells to biosensors to anticorrosive coatings [10].

One characteristic CP is polypyrrole (PPy), which also serves as the focus of this study. CPs formed from pyrrole have gained particular interest due to their high conductivity, processability, stability, and promising mechanical properties [10]. Additionally, PPy's biocompatibility has been demonstrated numerous times [11], [12], [13].

PPy offers a number of advantages over microfluidics. Through the application of electric potentials, CPs exchange ions with the surrounding solution. This allows PPy to act as a chemical actuator and alter the chemical composition of the bulk solution without the need for additional fluid input. Biological samples are sensitive to their environment, and the use of PPy minimizes physical disturbance of the sample. Finally, all testing could be completed in a single chamber, and LOC design could be simplified through the removal of microchannel arrays.

1.2.1 Ion Exchange in Polypyrrole

PPy reacts differently to ions depending on the electric field applied and the dopant used. For this study, the dopants used were para-toluene sulfonate (PTS), dodecyl sulfate (DS), and dodecylbenzenesulfonate (DBS). All dopants were large, sulfur-containing, negatively monovalent molecules. Once they imbed in the polymer backbone, their large size renders them immobile. Their negative charge balances with PPy's cationic backbone to form a neutrally charged polymer. For all the dopants used in this study, the resulting polymers exchange cations (specifically potassium ions K^+) with the solution. Therefore, PPy favors the ingress of cations into the polymer in its reduced state and the ejection of inserted cations when oxidized [14]. Two

phenomena occur during reduction: cations ingress to redox sites (faradaic response) and cations build up on the surface of the polymer (double layer effect). Ion ingress is driven by the combination of the potentials created by the electric field applied and the concretion gradient of cations between the bulk solution and the membrane [15]. Figure 1, below, depicts ion transport for PPy in its reduced and oxidized states.

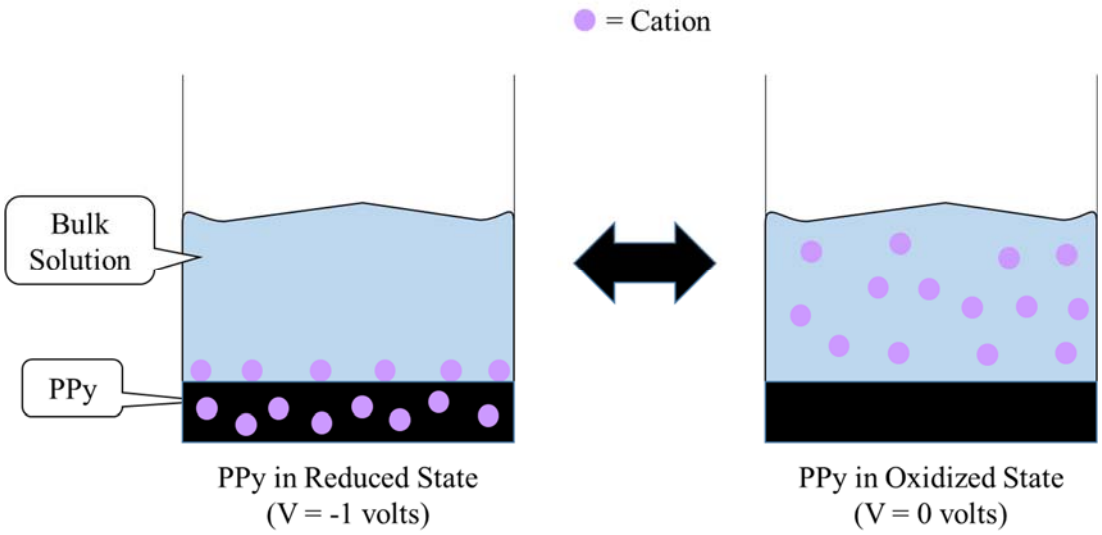

Figure 1: Ion exchange between bulk solution and PPy in reduced and oxidized states

A metric for quantifying ion transport in CPs is filling efficiency (calculated ion ingress divided by the theoretical maximum number of redox sites). Filling efficiency is a measure of a polymer's capacity to store cations. For polymers with the same deposited charge, a higher filling efficiency indicates that the polymer can intake and store a greater number of ions. The theoretical maximum number of redox sites (N_r) can be calculated from Equation 2, where Q_p represents charge deposited on the membrane during electropolymerization; η_p and η_c respectively represent the number of electrons produced and consumed during formation of a single polymer unit; and F represents the Faraday constant (96485.33289 $C \cdot mol^{-1}$). Filling efficiency can be calculated from

Equation 3, where ψ represents the filling efficiency and Q_r represents the maximum charge stored by the polymer during reduction [16].

$$N_r = \frac{Q_p}{(\eta_p - \eta_c)F} \tag{2}$$

$$\psi = \frac{Q_r}{N_r} = \frac{Q_r(\eta_p - \eta_c)F}{Q_p} \tag{3}$$

1.3 Objectives

The overall objectives of this project are to:

- Calculate filling efficiency and other parameters for PPy formed with varying dopants and charge densities to quantify and compare polymer performance
- Further scientific understanding of PPy and its potential for use in biological research

1.4 Overview of Thesis

The following chapter discusses the methods used to conduct this study, including sample fabrication and post-processing procedures. Chapter 3 presents experimental results and interpretation of those results. Finally, Section 4 summarizes the experiment and discusses its possible expansions. References are included at the end.

Chapter 2: Methodology

Chapter 2 contains the procedures necessary to replicate this experiment. This study explores the effect of various dopants (PTS, DS, and DBS) on the properties of PPy, and this chapter thus begins with a discussion of dopant morphology (Section 2.1) to familiarize the reader with the materials being used in polymer formation. Section 2.2 outlines the process for fabricating membrane substrates, which form the base of the working electrodes. A three-electrode configuration was used for all electrochemical processes. To complete the working electrodes, PPy must first be deposited onto the surface of the electrodes through electropolymerization. Sensor tests were conducted in 100 mM potassium chloride (KCl) using chronoamperometry. Before testing, each membrane was equilibrated in 100 mM KCl to ensure the membrane had reached a steady state response. Electropolymerization, characterization, and sensor testing are covered in Section 2.3. Data collected during the experiments then went through post-processing, and all post-processing procedures, including the methods used to calculate filling efficiency, are included in Section 2.4.

2.1 Dopant Morphology

The overall properties of PPy are greatly dependent on the dopant assimilated into the polymer during its synthesis. For this reason, three dopants (PTS, DS, and DBS) with similar morphologies were selected for use in this study, and the structural formula of each these dopants can be seen in Figure 2.

Structural Formula	Dopant
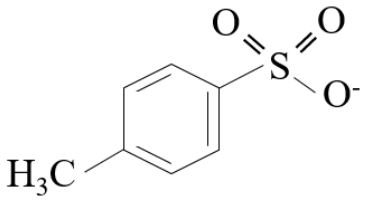	**PTS**
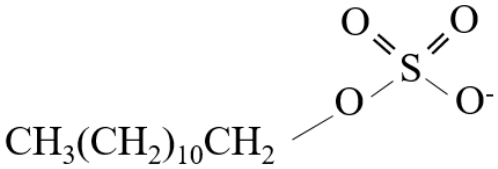	**DS**
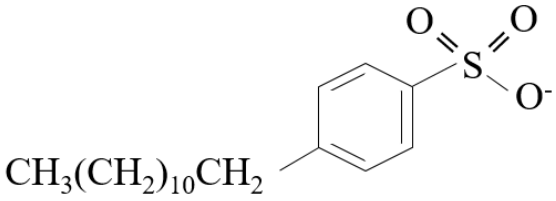	**DBS**

Figure 2: Structural formulas of p-toluenesulfonate (PTS), dodecyl sulfate (DS), and dodecylbenzenesulfonate (DBS)

All three dopants consist of a polar head composed of a sulfur-containing group (sulfate for DS and sulfonate for PTS and DBS). The polar head promotes strong interactions with the cationic PPy backbone, increasing the conductivity and ion affinity of the polymers. Two structural features that may further increase conductivity are increased order and amphiphilicity.

From Warren *et. al.*, order in PPy can be ranked as follows: PPy(PTS) ≥ PPy(DBS) > PPy(DS). PPy(PTS) was found to have the highest conductivity of the three, and despite order in PPy(PTS) and PPy(DBS) being nearly equal, PPy(DBS)'s conductivity was a magnitude lower

than PPy(PTS) [17]. According to findings by Raudsepp *et. al.*, of the aromatic sulfonate dopants tested by them, PPy(PTS) had the densest packing. Packing is dependent on dopant and polymer chain interactions – themselves partially a function of charge distribution. Charge distribution in PTS is highly uneven, with alternating positive and negative partial charges and concentrated areas of negative partial charge. These areas of concentrated negative charge may lead PTS to form a stronger interaction with the positively charged PPy chains than found in either PPy(DS) or PPy(DBS) and thus cause the dense packing observed in PPy(PTS) [18]. While this structure may increase conductivity, dense packing can hinder ion transport.

Large, amphiphilic surfactant molecules interact with pyrrole to form polymers with exceptional electrochemical and mechanical properties. Their size combined with their amphiphilicity renders them immobile in the polymer backbone. The polar head interacts with the charged backbone while the long, nonpolar tails form additional interactions with the neutral polymer matrix [14]. While all three dopant molecules presented are large and amphiphilic, PTS has a much shorter hydrocarbon tail than DS and DBS, which results in a smaller dipole moment and thus weaker tail – polymer matrix interactions. Packing is also expected to be less dense in PPy(DS) and PPy(DBS) due to steric effects.

2.2 Electrode Fabrication

Samples were prepared following the general procedure from [15]. Each substrate consisted of a polycarbonate track etch (PCTE) membrane filter (Isopore, 10 μm TCTP, Millipore) sputtered with a 25 nm thick layer of gold. To form the working electrode, silver wire was attached to the bottom of the substrate with silver ink. A layer of epoxy was then applied over the silver

wire and silver ink to prevent their participation in electrochemical processes [15]. Each sample had an effective area of 0.31 cm^2. A prepared substrate can be seen in the top image of Figure 3.

For all electrochemical processes, gold and silver / silver chloride were used as the counter electrode and reference electrode respectively. The same silver wire used in fabricating the working electrodes was immersed in sodium hypochlorite (reagent grade, 10 – 15% available chlorine) for 20 minutes to form silver / silver chloride, which was then used as the reference electrode.

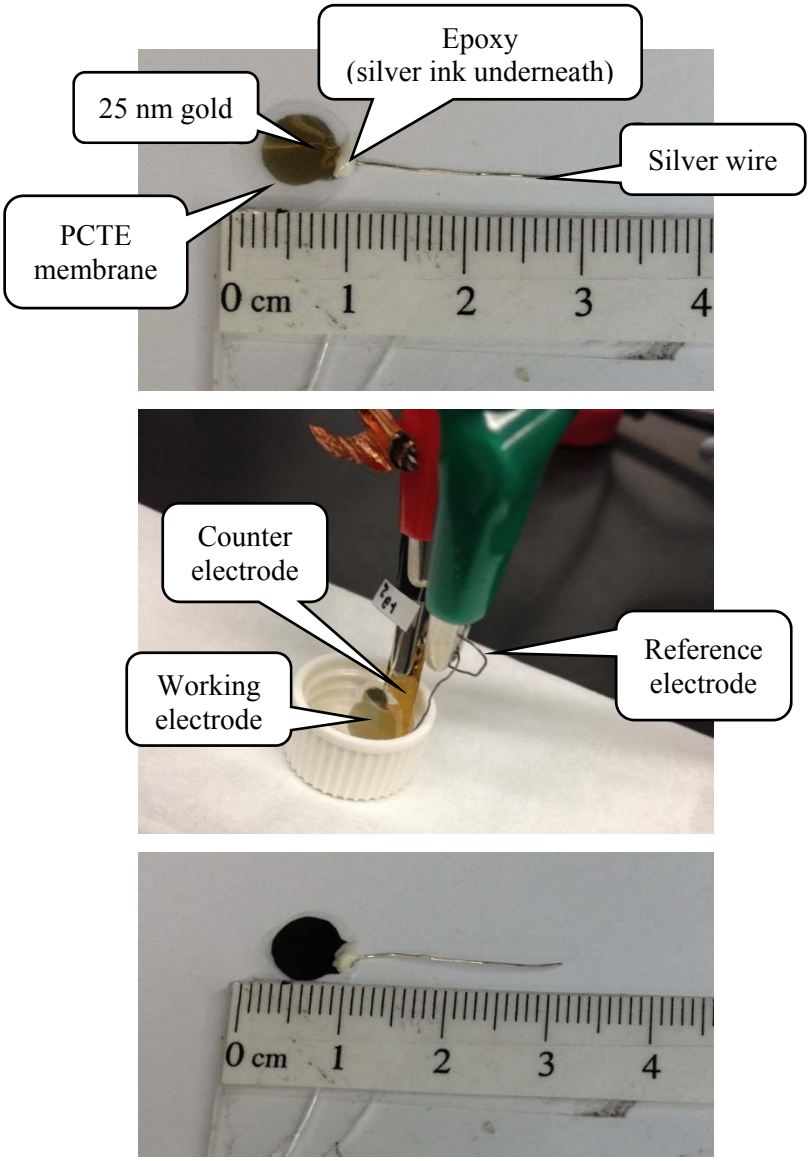

Figure 3: Assembled substrate (top), experimental setup (middle), and completed sensor (bottom)

2.3 Electropolymerization and Membrane Characterization

Polymerization solutions were prepared in deionized water (resistivity 18.2 MΩ·cm) with 100 mM pyrrole monomers (reagent grade, 98%) and 100 mM dopant salt (tetraethylammonium p-toluenesulfonate (97%), sodium dodecyl sulfate (99%), or sodium dodecylbenzenesulfonate (technical grade)). All chemicals were purchased from Sigma Aldrich. Potentiostatic electropolymerization with a three-electrode configuration was conducted at 0.55 V using a PARSTAT-4000 to form PPy onto the exposed gold until the desired charge density was achieved (0.4 C/cm^2, 0.8 C/cm^2, or 1.2 C/cm^2). After polymerization, each membrane was rinsed with deionized water and dried.

Membranes were equilibrated by cyclic voltammetry (-1.0 V to 0 V for PPy(PTS) and PPy(DBS), -1.0 V to 0.2 V for PPy(DS)) in 400 μL of 100 mM potassium chloride (KCl). The difference in potential range for PPy(DS) was due to unfamiliarity with the dopant, so a more conservative range was selected to avoid overoxidation of the membranes. Membranes were cycled until two consecutive cycles were equivalent; this preconditions the polymer to behave in a steady state manner that encourages identical ion exchange for subsequent redox events. Scan rate was 50 mV/s. For experiments to determine filling efficiency, each electrode then underwent chronoamperometry (-1 V reduction voltage, 0 V oxidation voltage). Figure 3 shows the experimental setup used for both polymerization and characterization as the middle image, and the bottom image of Figure 3 features a completed PPy sensor.

A total of 27 membranes were created with various dopants and charge densities. Table 2 summarizes the characteristics of each set of membranes.

Table 2: Characteristics of each PPy sensor

Sample	Quantity	Dopant	Charge Density (C/cm^2)
A, B, C	3	PTS	0.4
D, E, F	3	PTS	0.8
G, H, I	3	PTS	1.2
J, K, L	3	DS	0.4
M, N, O	3	DS	0.8
P, Q, R	3	DS	1.2
S, T, U	3	DBS	0.4
V, W, X	3	DBS	0.8
Y, Z, AA	3	DBS	1.2

2.4 Data Analysis

Data from the PARSTAT-4000 were exported to Microsoft Excel and then imported into MATLAB for analysis. The cyclic voltammograms (CVs) and chronoamperograms (CAs) for each sensor were plotted. As filling efficiency is a function of the charge removed from the bulk solution, working with charge data was preferable to using the current data obtained directly from CAs. Current data from the CAs were therefore integrated with respect to time to calculate charge at the working electrode. Current-to-charge conversions were performed by the PARSTAT-4000, and chronocoulograms for each sensor were also plotted. Characteristic features of PPy CVs and chronocoulograms are shown in Figure 4 and Figure 5 respectively.

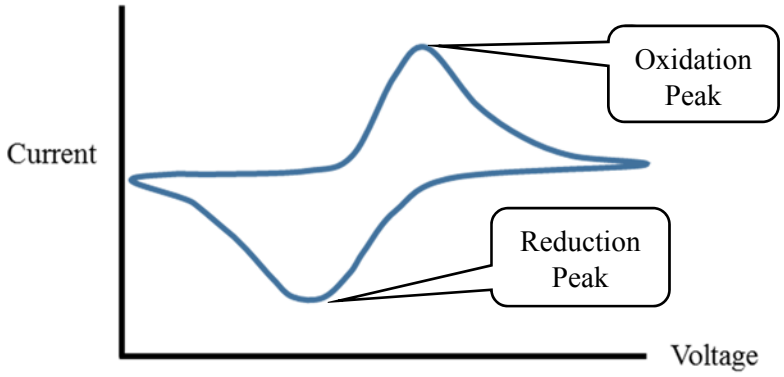

Figure 4: Characteristic features of cyclic voltagramm for PPy

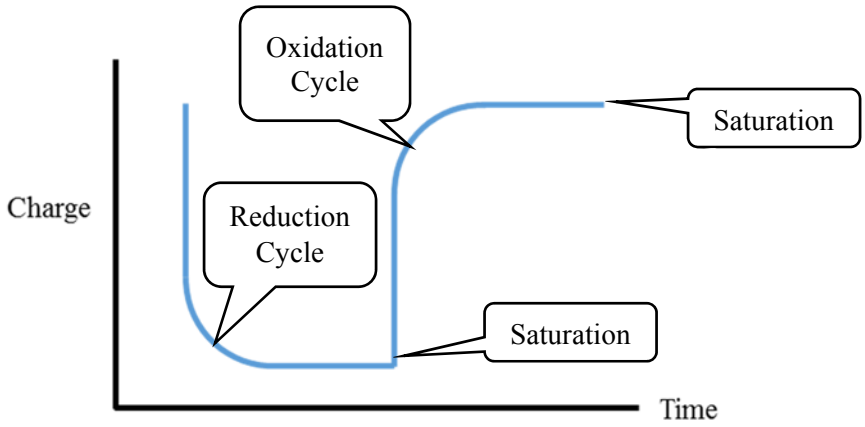

Figure 5: Characteristic features of chronocoulogram for PPy

From the CV data, the reduction and oxidation peaks of every cycle were determined and plotted. To calculate filling efficiency, the amount of ions removed from solution by the polymer (Q_r) first had to be calculated. This was done by applying a second-order exponential fit (Equation 4 below) to the reduction cycles of the chronocoulograms [15]. In Equation 4, q(t) represents charge as function of time t; k_1 represents the first residue; k_2 represents the second residue; k_3 represents the third residue; $\frac{1}{\tau_1}$ represents the first pole; $\frac{1}{\tau_2}$ represents the second pole; and $\frac{1}{\tau_3}$ represents the third pole.

$$q(t) = k_1 e^{\frac{t}{\tau_1}} + k_2 e^{\frac{t}{\tau_2}} + k_3 e^{\frac{t}{\tau_3}} \quad (4)$$

The poles and residues for each reduction cycle were extracted from the fit data and plotted. The first two terms of Equation 4 were then calculated from the fit data. The first term, $k_1 e^{\frac{t}{\tau_1}}$, represents the faradaic response while the second term, $k_2 e^{\frac{t}{\tau_2}}$, is the double layer response. The third term, $k_3 e^{\frac{t}{\tau_3}}$, represents the potential step input, and as the step input is not indicative of an ion transport phenomenon, the third term was disregarded for all analyses. Q_r, the total cations stored, was determined by taking the absolute value of the difference between the maximum and minimum values of $k_1 e^{\frac{t}{\tau_1}}$. Q_r was converted to moles and entered into Equation 3 to find the filling efficiency of each reduction cycle.

Chapter 3: Results and Discussion

This chapter presents and interprets the results of this project. In Section 3.1, characteristic examples of CVs per dopant and charge density are shown along with redox peaks derived from every CV cycle (Section 3.1.1). Section 3.2 contains the corresponding chronocoulograms derived from the CAs for each sample included in Section 3.2. Second-order exponential fits were applied to each reduction cycle in the chronocoulogram, but only the fit applied to the first reduction is shown as all fits within the same chornocoulogram were similar. Data from these fits were used to conduct pole-residue analyses and calculate filling efficiencies, and results for every sample are available in Sections 3.2.1 and 3.2.2 respectively.

3.1 Cyclic Voltammograms

CVs show current at the working electrode as a function of the potential at the working electrode. Potential is ramped linearly against time and cycles within a user-defined range. For PPy(PTS) and PPy(DBS), potential range was between -1 V and 0 V; for PPy(DS), potential range was from 0 V to -0.2 V. The points on a CV represent the instantaneous rate of ion transport at that particular potential.

A typical CV for a polymer with reversible cation exchange has two defined peaks. The reduction peak occurs at the point where current is at a minimum, and the oxidation peak occurs at the point where current is at a maximum. These peaks represent the maximum instantaneous rates of cation ingress (reduction peak) or egress (oxidation peak).

Figures 6, 7, and 8 show example CVs for PPy(PTS), PPy(DS), and PPy(DBS) respectively at each charge density.

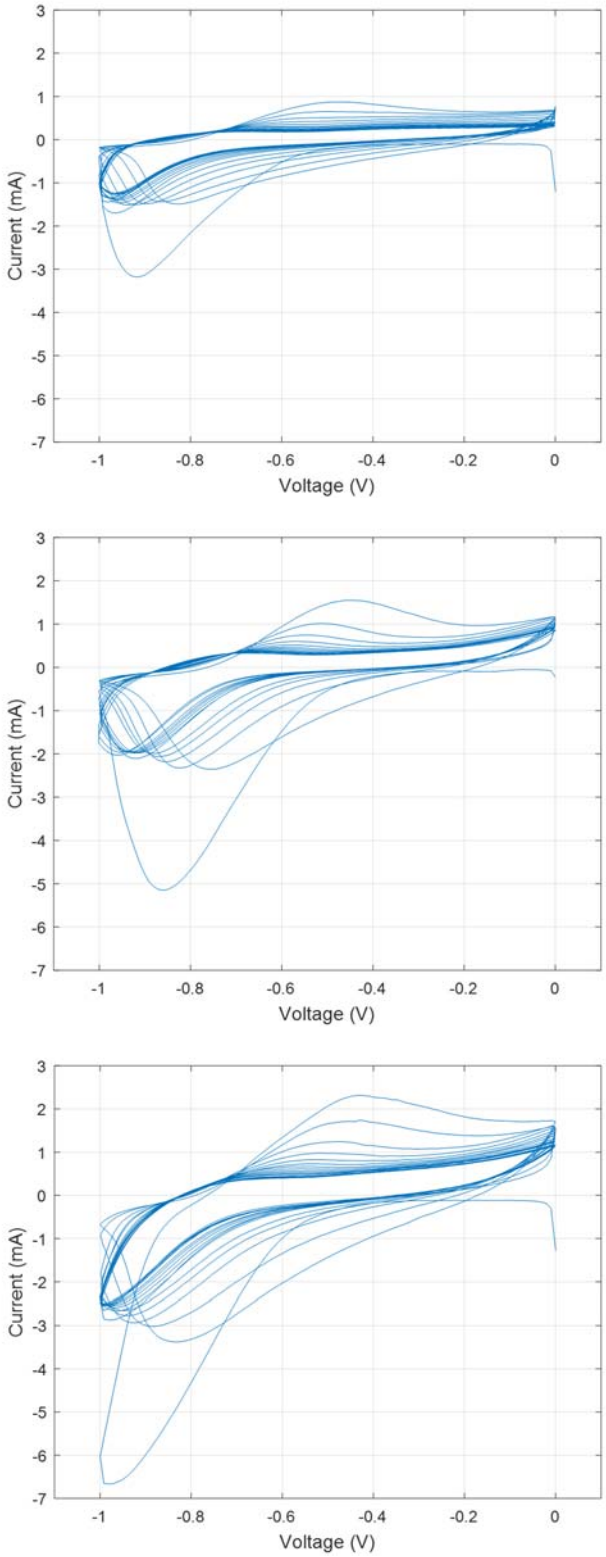

Figure 6: Cyclic voltammograms for PPy(PTS)

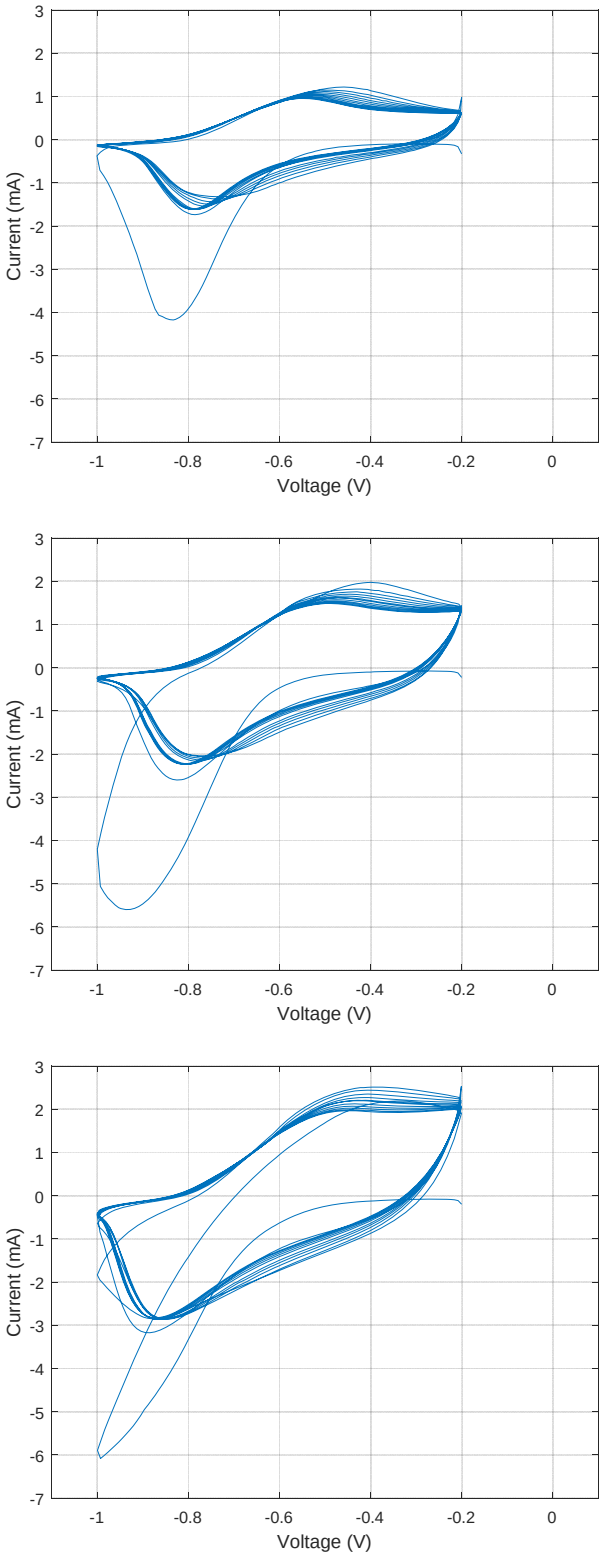

Sample L

0.4 C/cm^2

Sample M

0.8 C/cm^2

Sample P

1.2 C/cm^2

Figure 7: Cyclic voltammograms for PPy(DS)

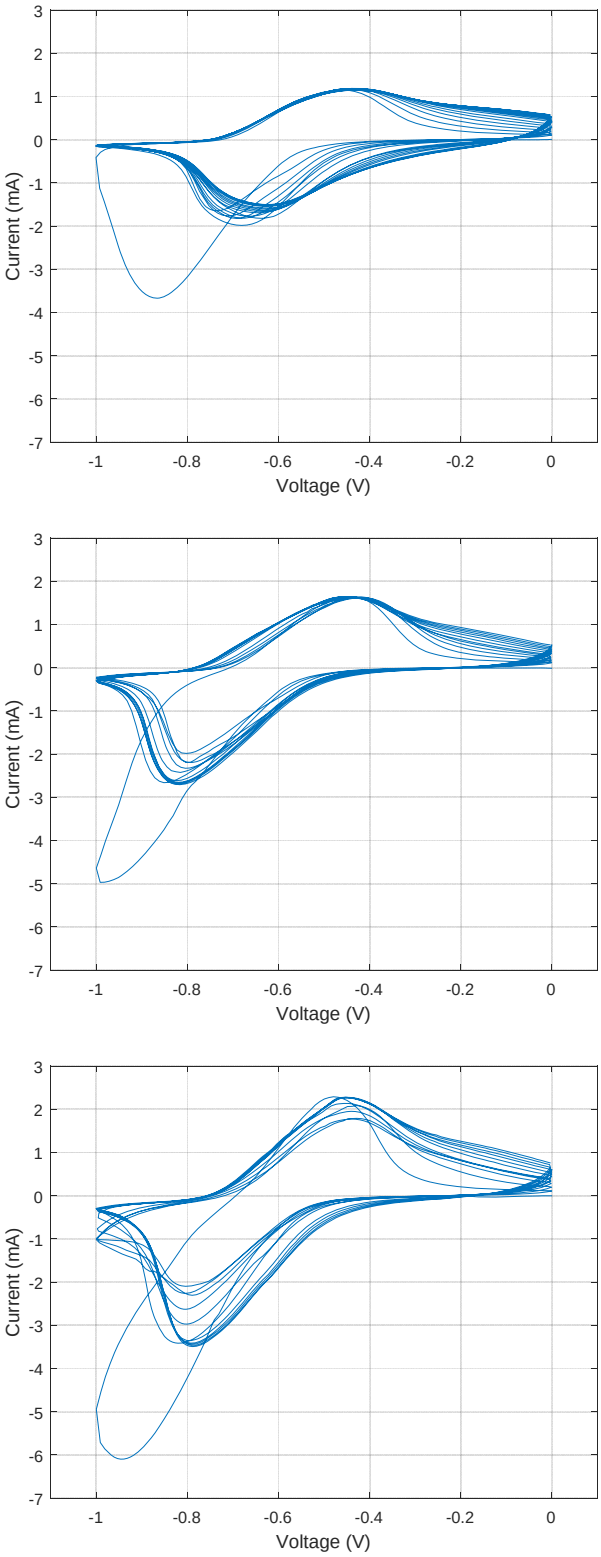

Figure 8: Cyclic voltammograms for PPy(DBS)

From Figures 6, 7, and 8, at each charge density, the first cycles of PPy(PTS), PPy(DS), and PPy(DBS) have approximately the same current at their reduction and oxidation peaks. While PPy(PTS) displays reversible behavior for the first one or two cycles, the oxidation currents gradually decline until no peak is present. As the oxidation peaks decrease, fewer and fewer cations are being released back into solution. Fewer cations then can ingress into PPy(PTS) when the polymer is reduced, and similarly, reduction peaks decrease every cycle until the peak disappears. No redox peaks are present at equilibrium, and ion exchange has become irreversible.

PPy(DS) and PPy(DBS) maintain their redox peaks, although redox peaks for PPy(DS) are broader than corresponding peaks for PPy(DBS). Current drops sharply before and after redox peaks in PPy(DBS). Diffusion of ions is therefore rapid near the peaks but relatively slow elsewhere. In PPy(DS), current drop around reduction and oxidation peaks is more gradual, especially at potentials greater than the oxidation peak.

For all PPy variants, current increases with increasing charge density. As charge density increases, more PPy has to be deposited during electropolymerization, leading to the creation of thicker membranes. Thicker membranes have a greater number of available redox sites for ion ingression, and as charge stored in the membrane increases, so too does its current.

3.1.1 Reduction and Oxidation Peaks

Figures 9, 10, and 11 feature the redox peaks grouped by PPy variant from every PPy(PTS), PPy(DS), and PPy(DBS) cycle respectively. Figure 12 shows redox peaks measured from every CV cycle and across all dopants.

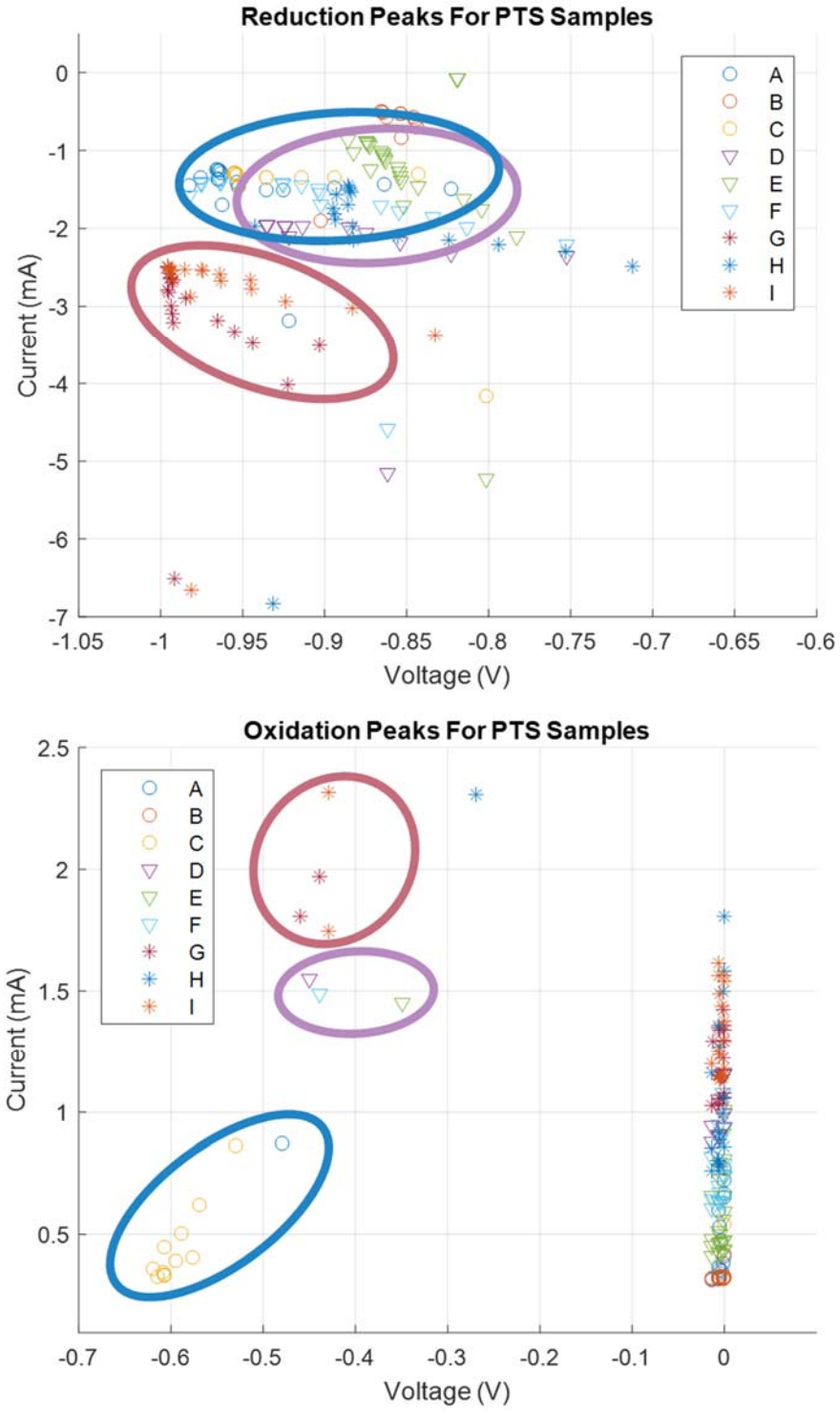

Figure 9: Reduction and oxidation peaks for PPy(PTS)
Legend refers to the sample ID established in Table 2. Outlined regions indicate concentrations of samples of the same charge density (blue = 0.4 C/cm^2, purple = 0.8 C/cm^2, red = 1.2 C/cm^2).

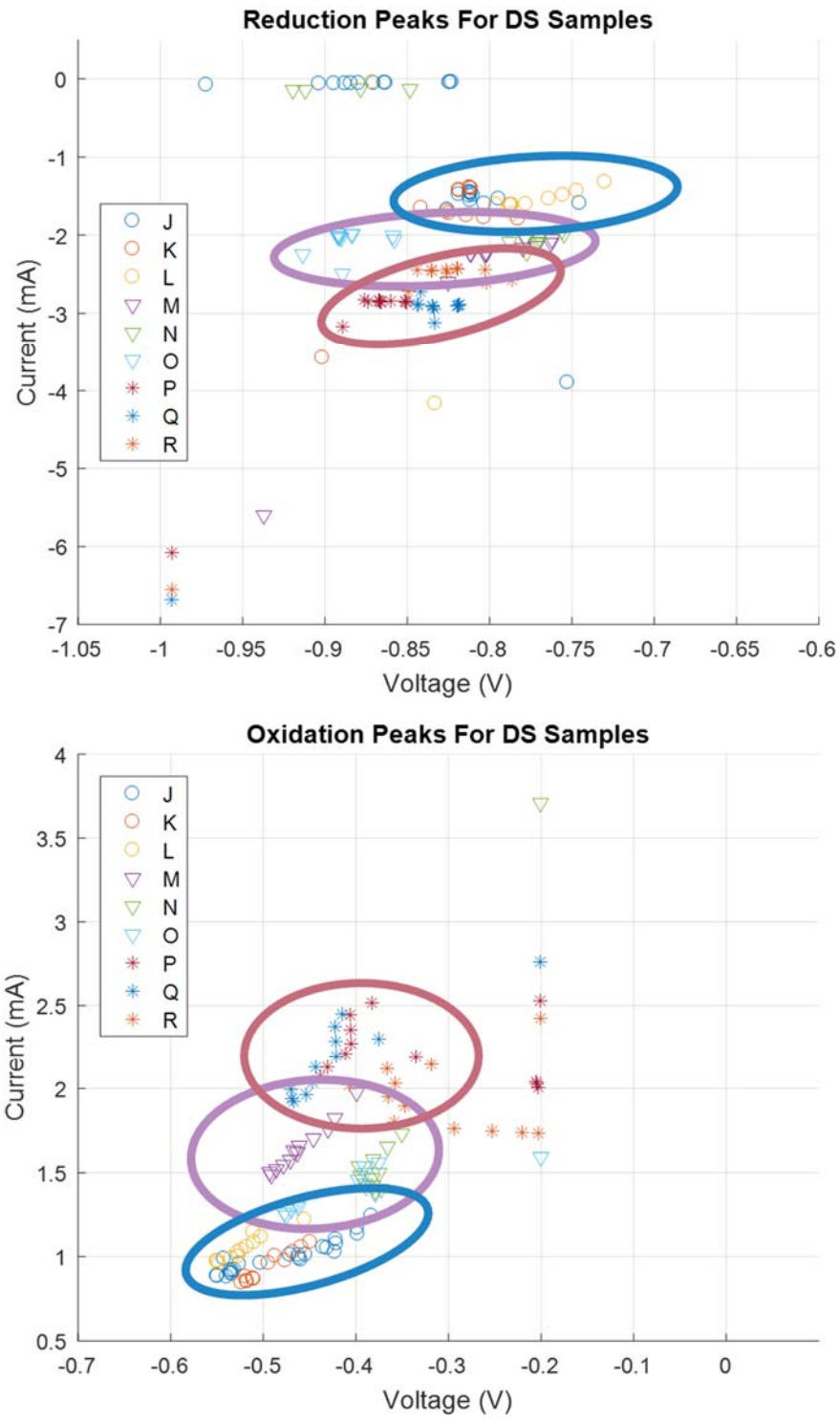

Figure 10: Reduction and oxidation peaks for PPy(DS)
Legend refers to the sample ID established in Table 2. Outlined regions indicate concentrations of samples of the same charge density (blue = 0.4 C/cm^2, purple = 0.8 C/cm^2, red = 1.2 C/cm^2).

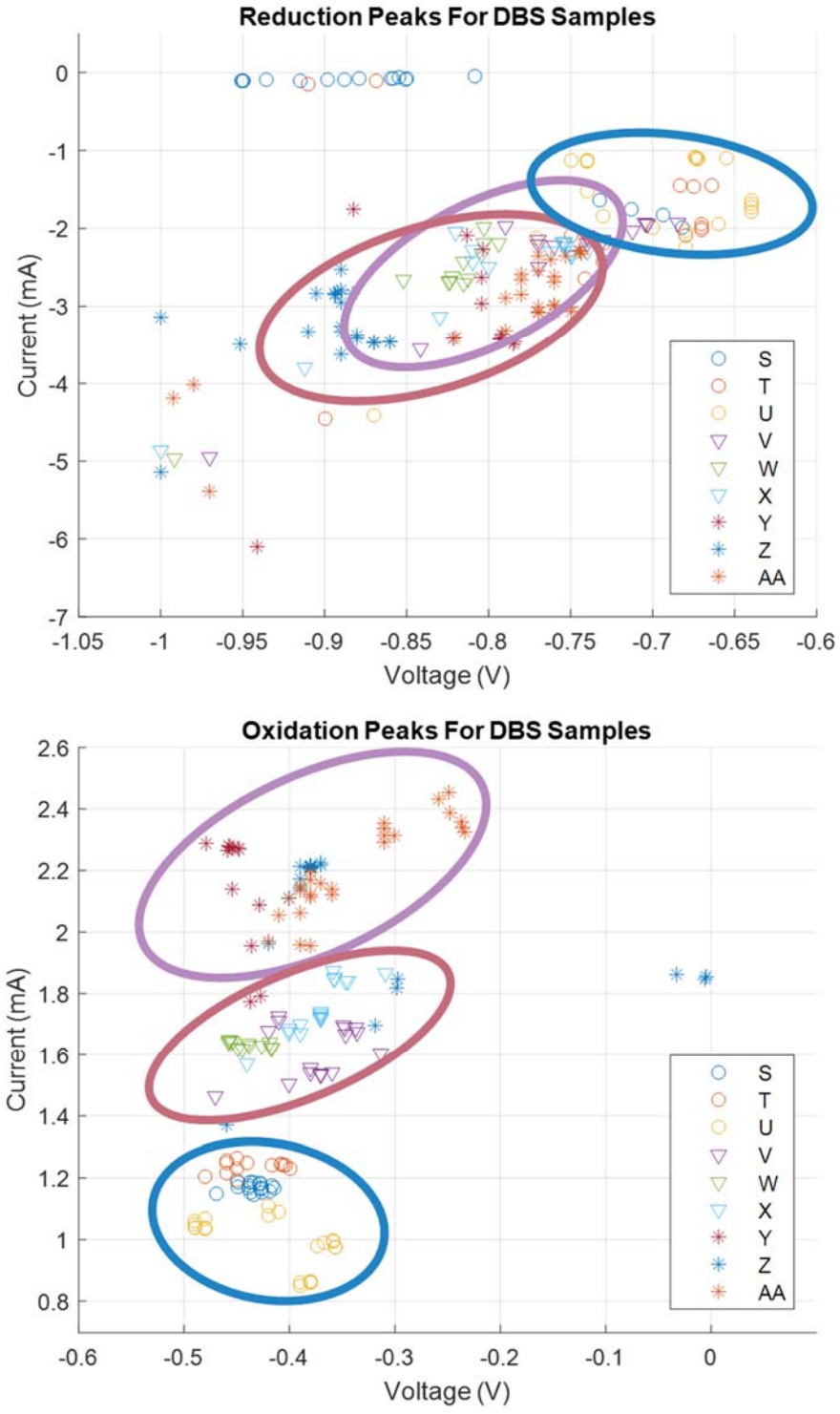

Figure 11: Reduction and oxidation peaks for PPy(DBS)
Legend refers to the sample ID established in Table 2. Outlined regions indicate concentrations of samples of the same charge density (blue = 0.4 C/cm^2, purple = 0.8 C/cm^2, red = 1.2 C/cm^2).

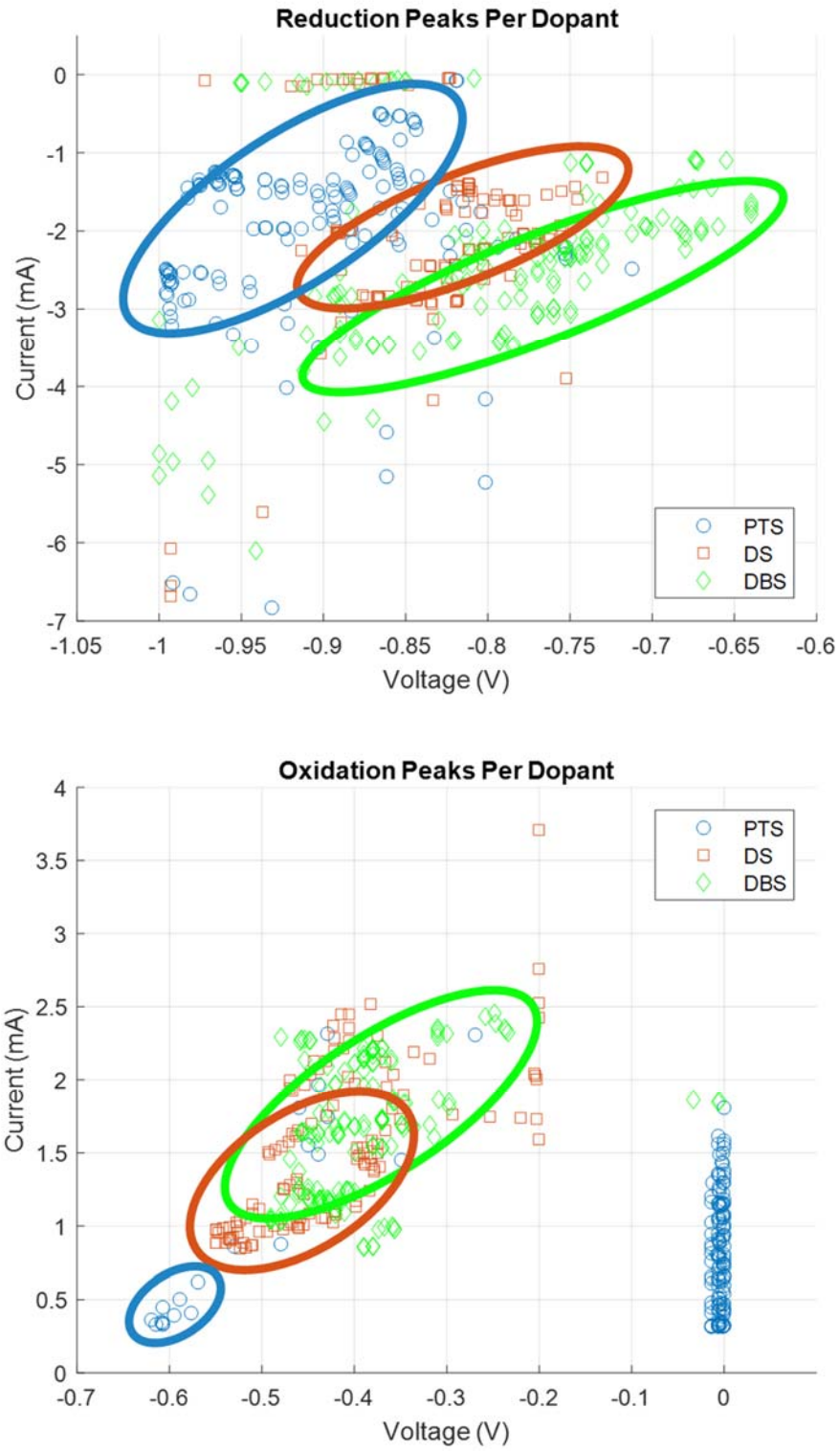

Figure 12: Reduction and oxidation peaks for all PPy membranes
Outlined regions indicate concentrations of samples with the same dopant (blue = PTS, red = DS, green = DBS).

For each PPy variant, redox peaks occurred at higher currents for membranes of higher charge densities. Membranes of higher charge density store more ions than membranes of lower charge densities due to the greater number of redox sites available in thicker polymers.

Per Figure 12, redox peak current was highest for PPy(DBS) followed by PPy(DS) and PPy(PTS). PPy(DBS) has the greatest affinity for K^+, and the lateral distribution of PPy variants in Figure 12 reinforces this. PPy(DBS) has the most positive reduction potential and the largest oxidation potential, so of the three, it is the easiest to reduce (ingress K^+) and most difficult to oxidize (egress K^+).

The irreversibility of ion transport in PPy(PTS) can be detected from the concentration of oxidation peaks at the edge of the potential range. If all oxidation peaks were located there, then it could be an indication that the potential range needs to be expanded. However, as a few oxidation peaks were recorded (primarily grouped around -0.6 V) not at the potential limit, then irreversibility becomes a more plausible explanation.

3.2 Chronocoulograms

CAs record current at the working electrode as a function of time. They are produced by stepping the potential at the working electrode. Use of chronoamperometry allows membranes to be quickly cycled between their fully-reduced and fully-oxidized states. Complete reduction or oxidation typically occurs within the first 5 seconds of the potential step.

From the reduction state, the total charge removed from solution by the polymer can be calculated from the method previously described in Section 2.4. Therefore, rather than working directly with the current measured through chronoamperometry, integrating it with respect to time to calculate charge becomes advantageous.

Three reduction and oxidation cycles were completed per membrane. Figures 13, 14, and 15 show chronocoulograms for a membrane of each charge density for PPy(PTS), PPy(DS), and PPy(DBS) respectively. Additionally, each figure includes the second-order exponential fit discussed in Section 2.4 applied to the first reduction cycle of the respective membrane. The fit allows the faradaic and double layer responses to be separated. The double layer component is a result of cation attraction to the polymer in its reduced state. Cations line up on the surface of the membrane but do not ingress. All cation storage that occurs during reduction is therefore captured by the faradaic response.

Sample A (0.4 C/cm^2)

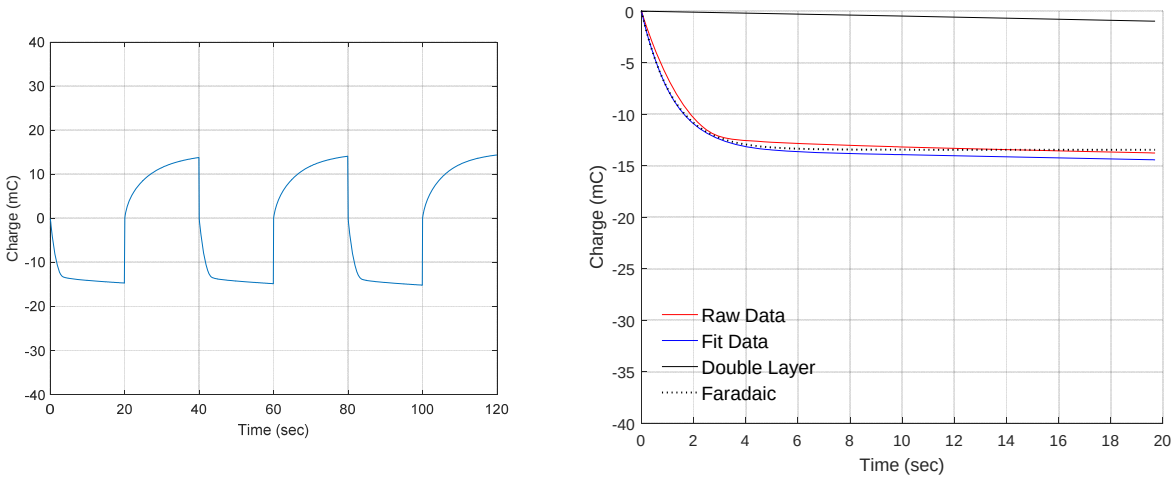

Sample D (0.8 C/cm^2)

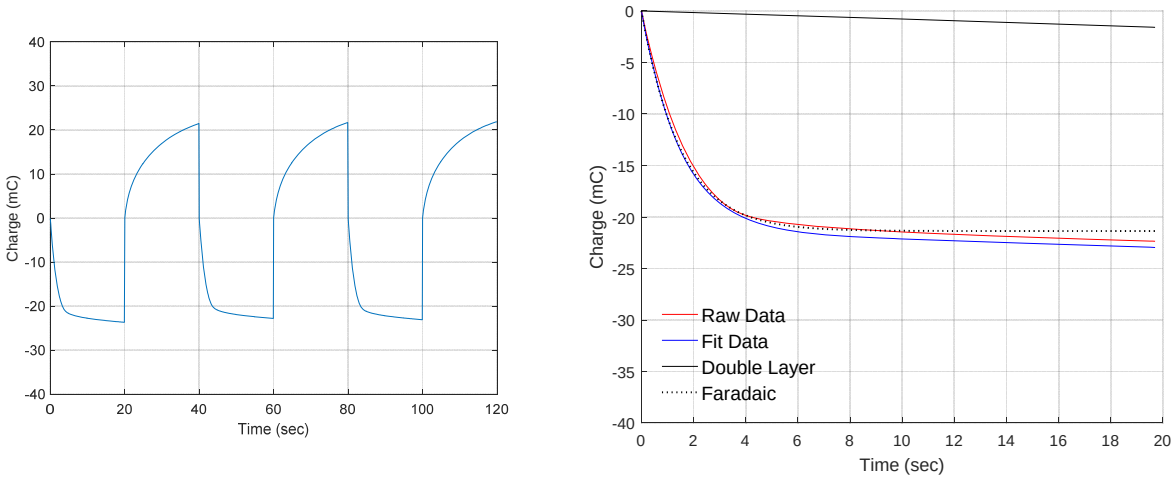

Sample I (1.2 C/cm^2)

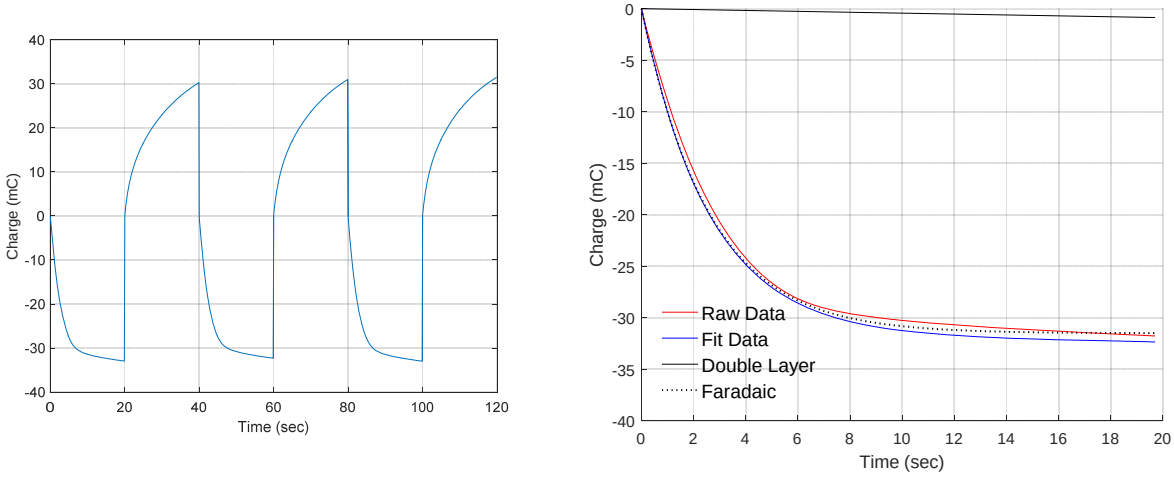

Figure 13: Chronocoulograms for PPy(PTS)
Second-order exponential fit applied to first reduction cycle.

Sample L (0.4 C/cm^2)

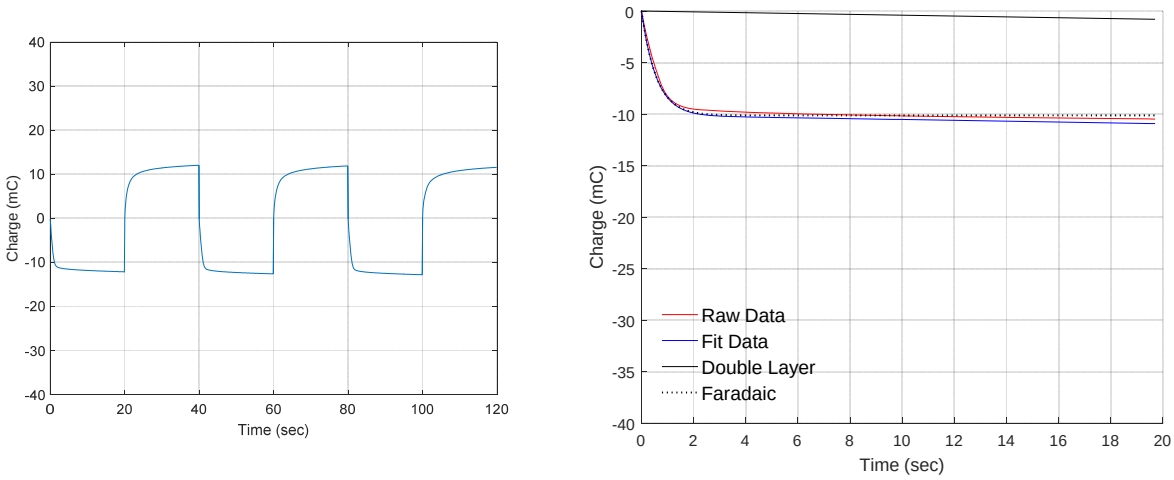

Sample M (0.8 C/cm^2)

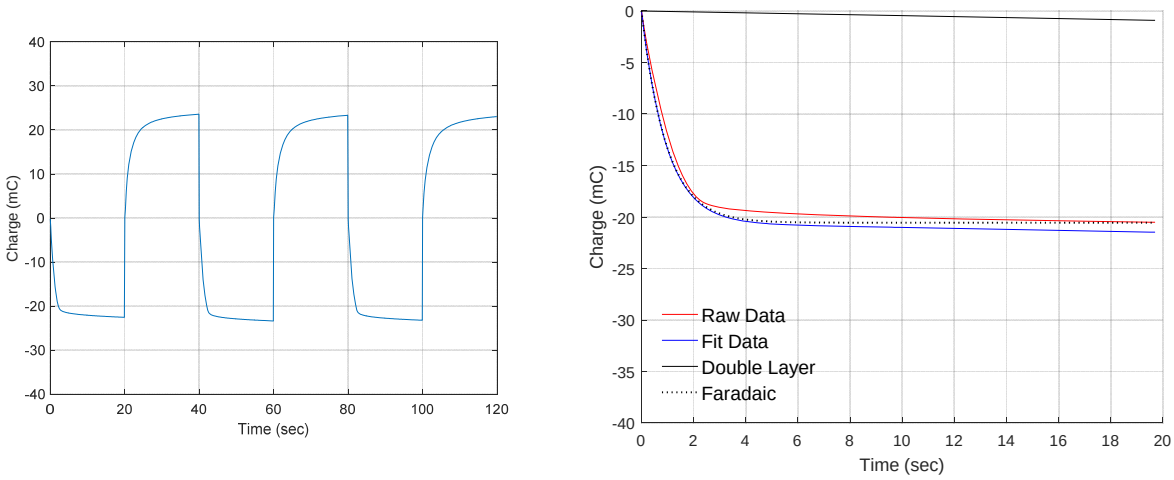

Sample P (1.2 C/cm^2)

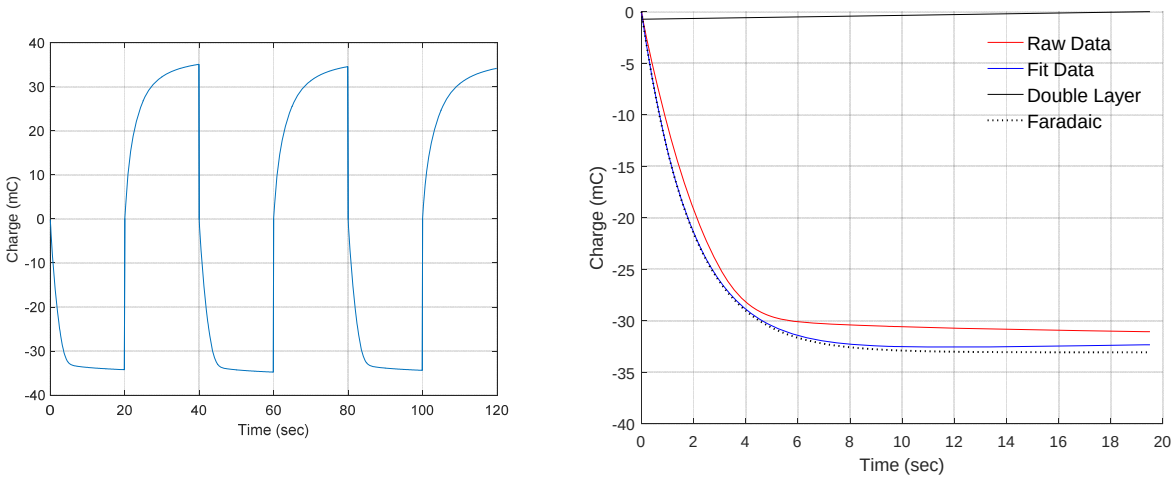

Figure 14: Chronocoulograms for PPy(DS)
Second-order exponential fit applied to first reduction cycle.

Sample S (0.4 C/cm^2)

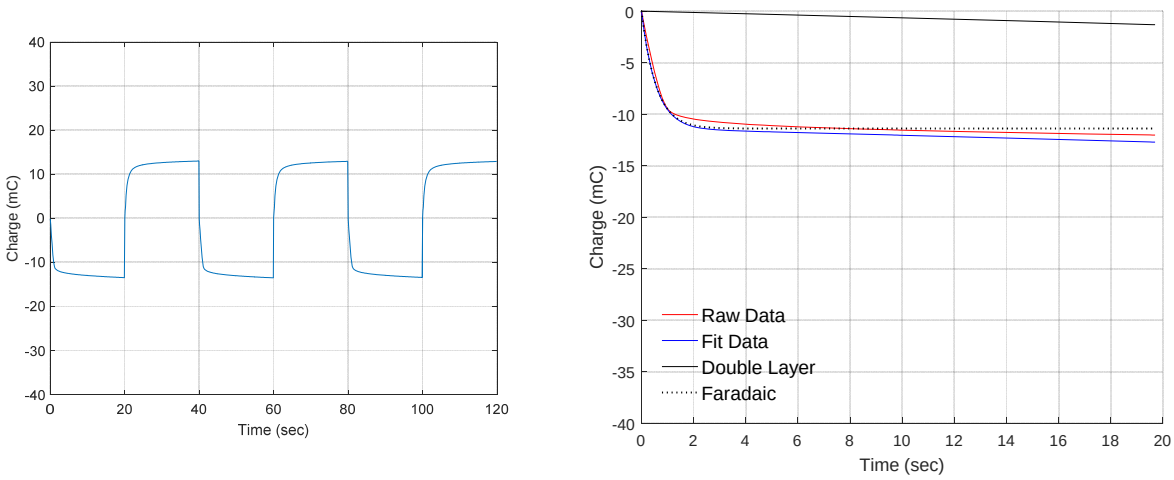

Sample W (0.8 C/cm^2)

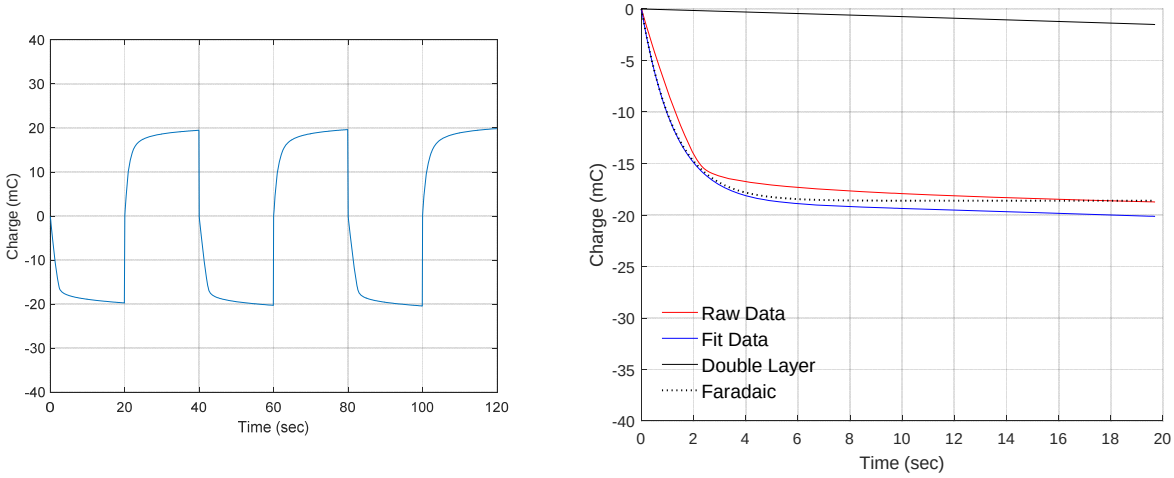

Sample Y (1.2 C/cm^2)

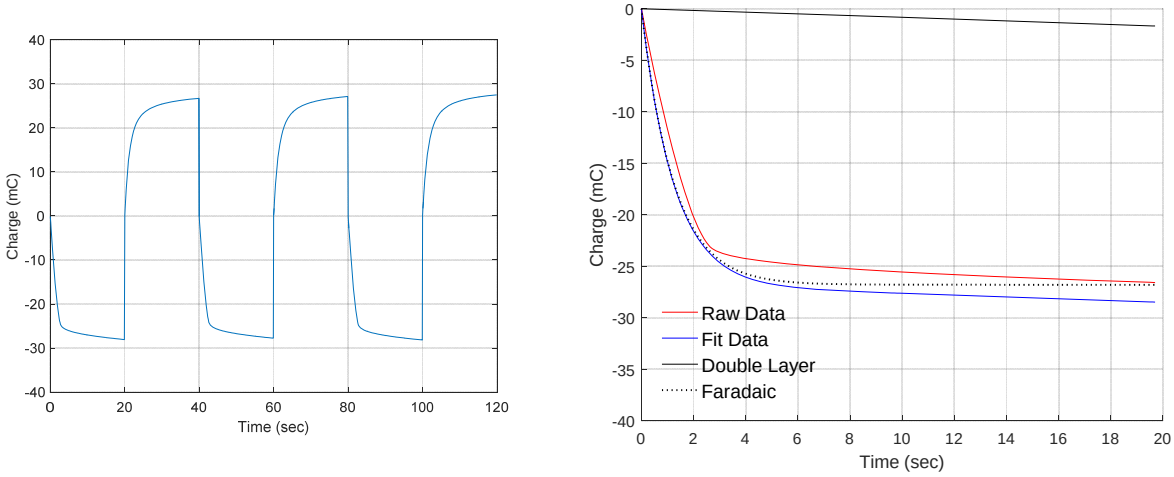

Figure 15: Chronocoulograms for PPy(DBS)
Second-order exponential fit applied to first reduction cycle.

As previously stated, membranes of higher charge densities possess a greater ion storage capacity. This is explicitly shown by Figures 13, 14, and 15, as charge increases proportional to charge density (approximately 10 mC at 0.4 C/cm^2, 20 mC at 0.8 C/cm^2, and 30 mC at 1.2 C/cm^2).

3.2.1 Poles and Residues

From [15], poles and residues obtained from a pole-residue analysis of transient reduction currents have been shown to relate to physical membrane properties and saturation kinetics respectively. From Equation 4, Pole 1 and Residue 1 compose the faradaic response, and Pole 2 and Residue 2 contribute to the double layer effect.

Figures 16, 17, and 18 feature the poles and residues of each PPy variant. Poles and residues were calculated from the second-order exponential fit applied to the reduction cycles of the chronocoulograms. Each membrane underwent three reductions, and thus, three sets of poles and residues are associated with each membrane. Figure 19 contains all the poles and residues as a function of dopant.

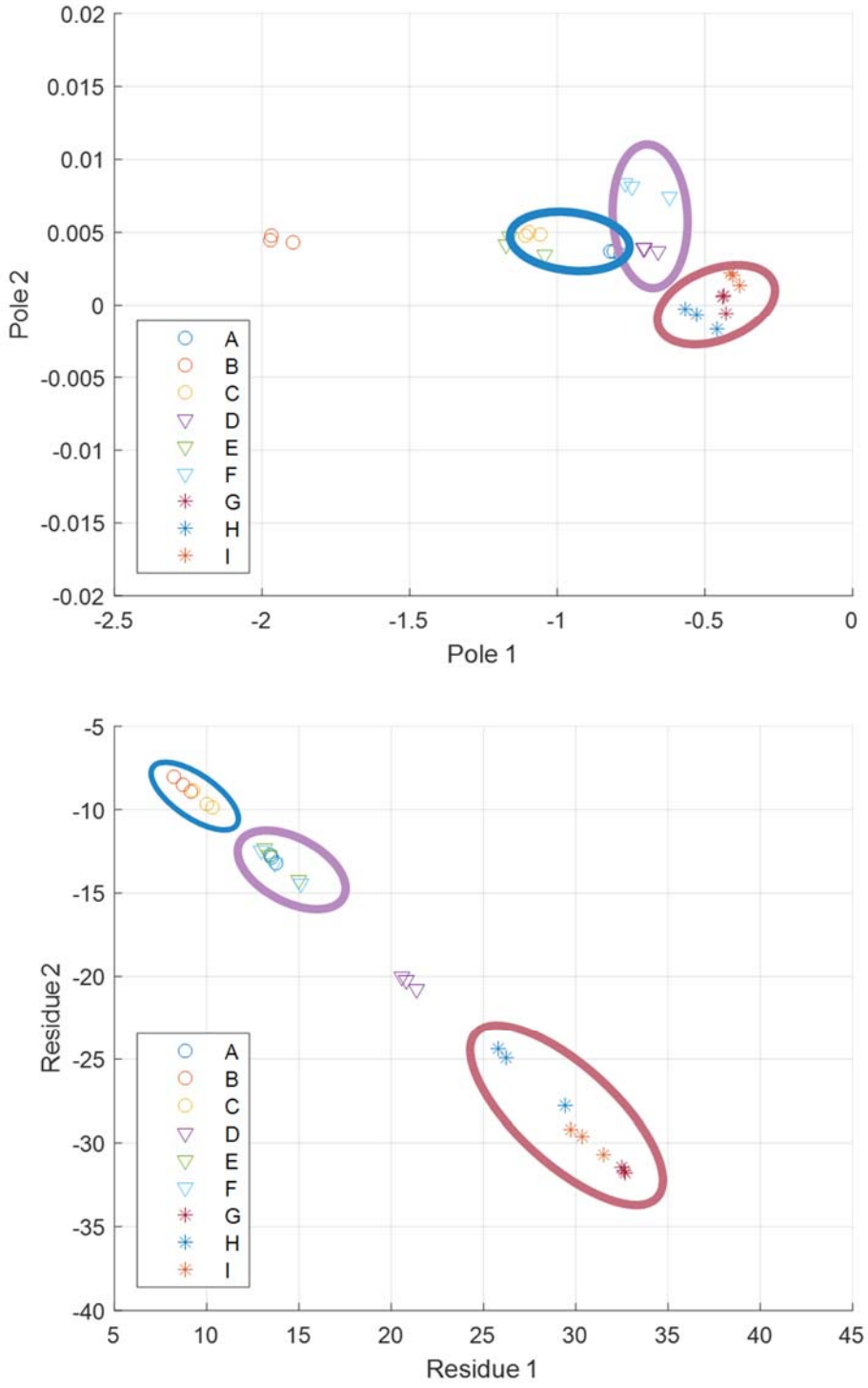

Figure 16: Poles and residues for PPy(PTS)
Legend refers to the sample ID established in Table 2. Outlined regions indicate concentrations of samples of the same charge density (blue = 0.4 C/cm^2, purple = 0.8 C/cm^2, red = 1.2 C/cm^2).

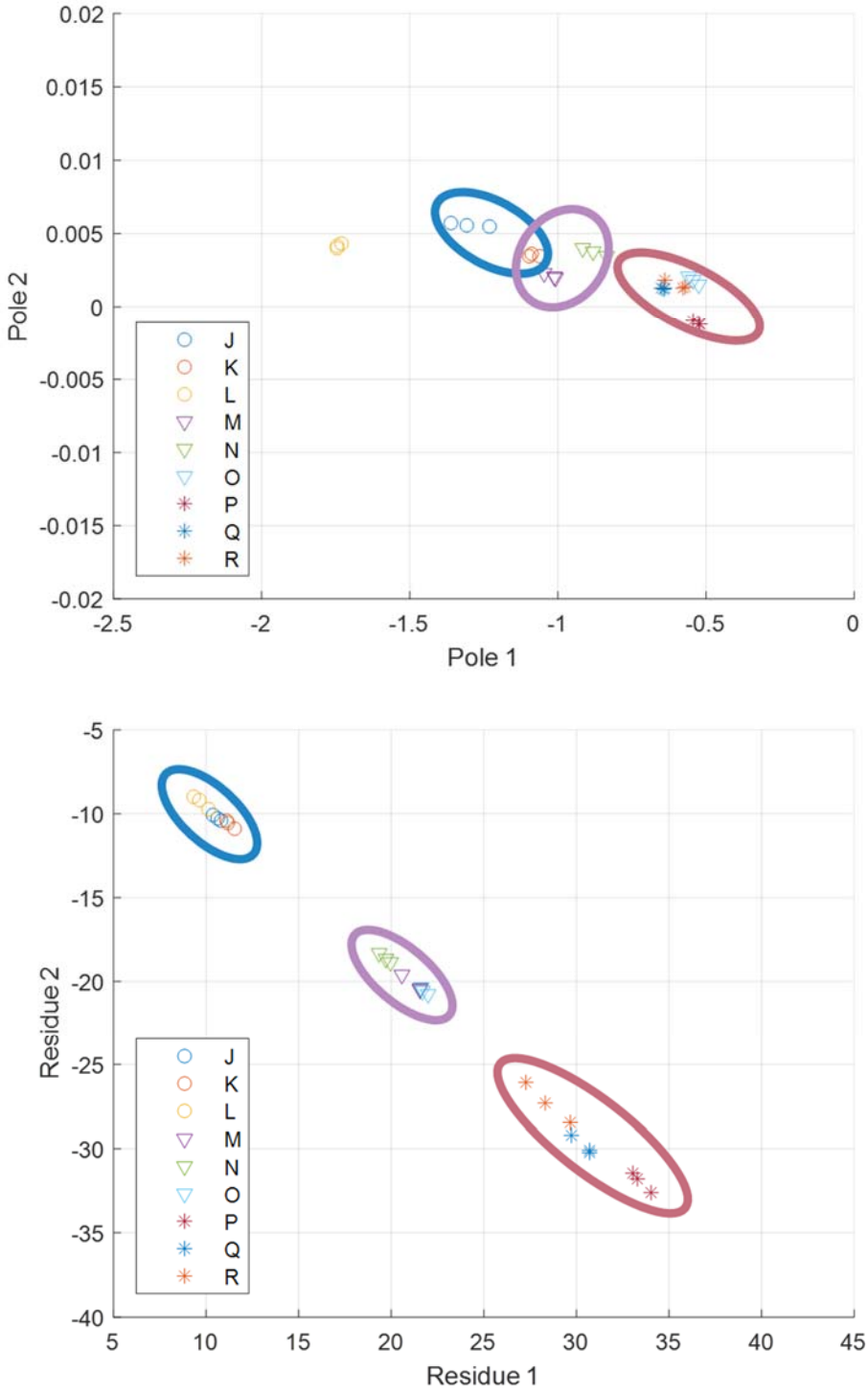

Figure 17: Poles and residues for PPy(DS)
Legend refers to the sample ID established in Table 2. Outlined regions indicate concentrations of samples of the same charge density (blue = 0.4 C/cm^2, purple = 0.8 C/cm^2, red = 1.2 C/cm^2).

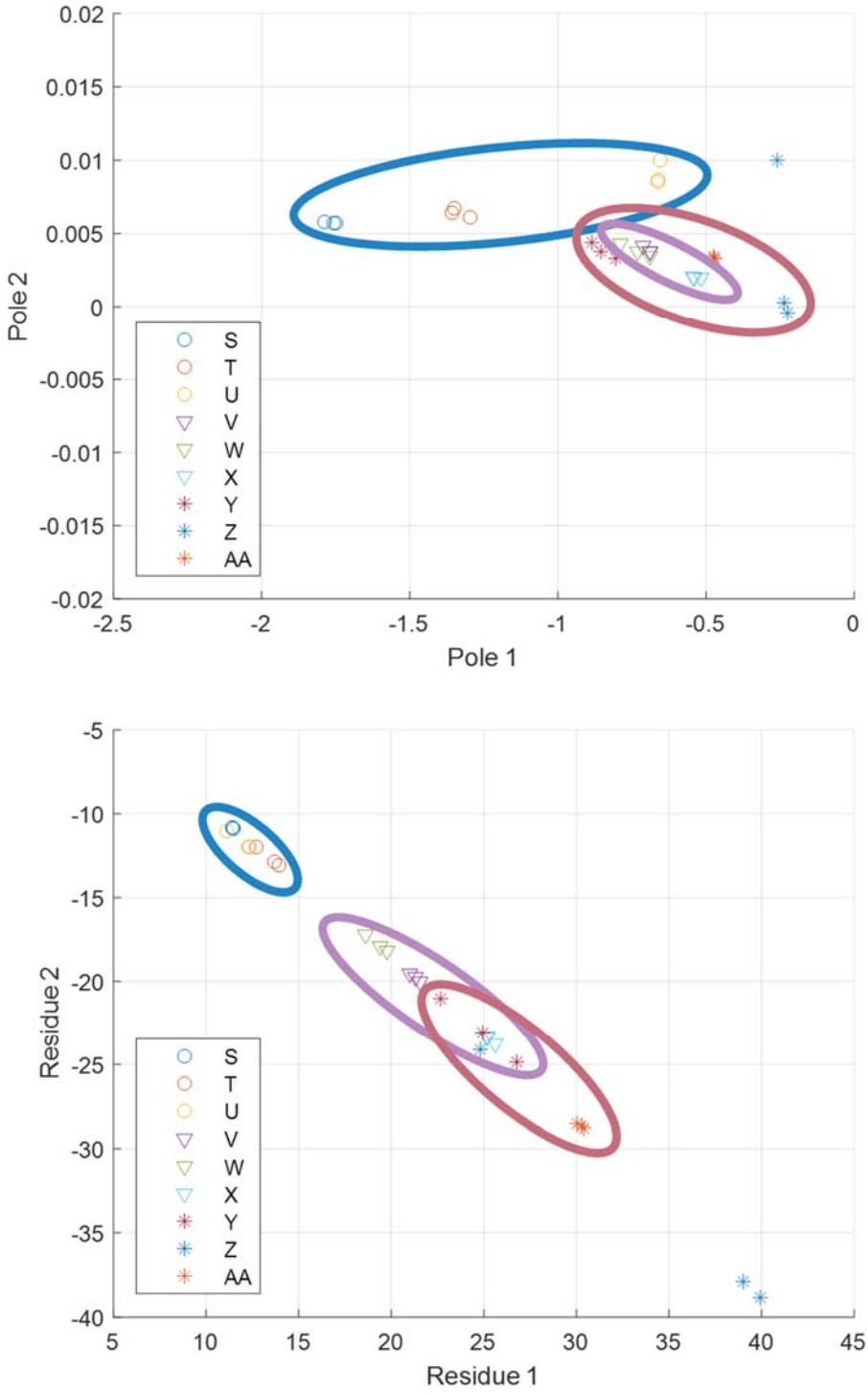

Figure 18: Poles and residues for PPy(DBS)
Legend refers to the sample ID established in Table 2. Outlined regions indicate concentrations of samples of the same charge density (blue = 0.4 C/cm^2, purple = 0.8 C/cm^2, red = 1.2 C/cm^2).

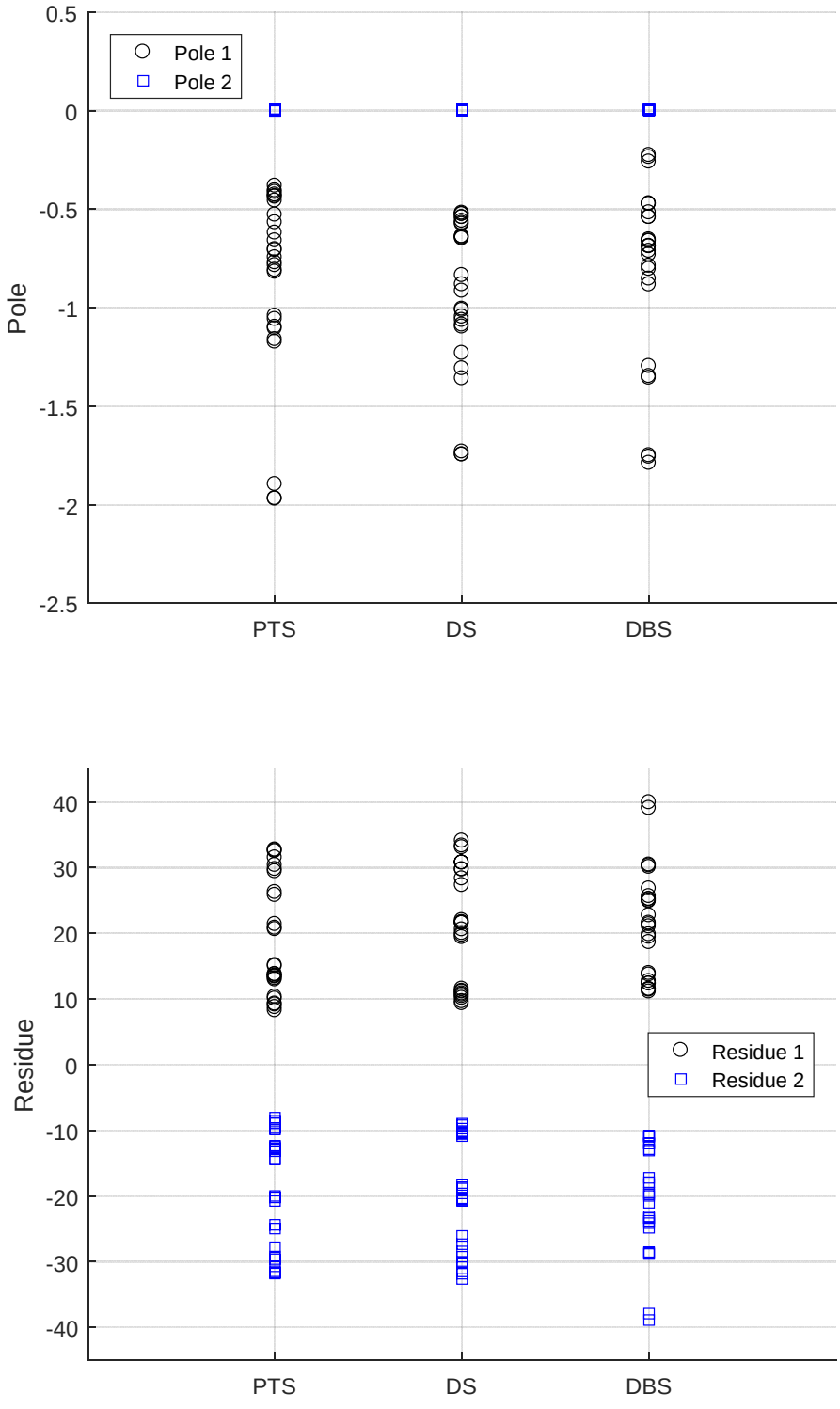

Figure 19: Poles and residues for all PPy membranes

From Figures 16 thorough 18, the magnitude of the poles and residues increases with increasing charge density. The residue plots suggest that the relationship between residues and charge density is linear for all PPy variants. Given the residue values of an unknown sensor, the charge density of the sensor could be extrapolated using this relationship.

Pole 2 is nearly zero for all membranes as expected; this is most evident from Figure 19. Pole 1 values range between -0.22 and -2.0. Variation in Pole 1 values is a measure of the reliability (structure and performance) of the components. While the spread of values for the membranes is higher than desired, some of the poles are visibly outliers. PPy(PTS) displays the tightest grouping with the majority of membranes between -0.4 and -0.8. PPy(DBS) comes in second with most samples within a range of -0.45 to -0.95, and PPy(DS) is most concentrated between -0.5 and -1.2.

3.2.2 Filling Efficiency

Filling efficiency represents a membrane's cation storage capacity, with higher filling efficiencies indicating greater storage capacity. As shown in Equation 3, filling efficiency is a function of the maximum charge stored by the polymer and the number of available redox sites. For each sample, filling efficiency was calculated using Equation 3. Results for samples doped with PTS, DS, and DBS are displayed below in Table 3, Table 4, and Table 5 respectively.

Table 3: Filling efficiencies for PPy(PTS) (Samples A through I)

Sample	Charge Density (C/cm^2)	Filling Efficiency (Reduction 1)	Filling Efficiency (Reduction 2)	Filling Efficiency (Reduction 3)	Filling Efficiency (Average Per Sample)	Filling Efficiency (Average Per Charge Density)
A	0.4	0.781	0.785	0.799	0.788	0.622
B	0.4	0.479	0.507	0.530	0.505	
C	0.4	0.599	0.582	0.537	0.573	
D	0.8	0.620	0.598	0.604	0.608	0.471
E	0.8	0.381	0.389	0.435	0.402	
F	0.8	0.439	0.398	0.378	0.404	
G	1.2	0.628	0.631	0.633	0.631	0.582
H	1.2	0.569	0.499	0.508	0.524	
I	1.2	0.609	0.588	0.575	0.591	

Table 4: Filling efficiencies for PPy(DS) (Samples J through R)

Sample	Charge Density (C/cm^2)	Filling Efficiency (Reduction 1)	Filling Efficiency (Reduction 2)	Filling Efficiency (Reduction 3)	Filling Efficiency (Average Per Sample)	Filling Efficiency (Average Per Charge Density)
J	0.4	0.604	0.617	0.628	0.616	0.611
K	0.4	0.669	0.651	0.644	0.655	
L	0.4	0.588	0.542	0.558	0.563	
M	0.8	0.597	0.626	0.625	0.616	0.607
N	0.8	0.580	0.573	0.562	0.572	
O	0.8	0.630	0.638	0.628	0.632	
P	1.2	0.659	0.645	0.640	0.648	0.596
Q	1.2	0.575	0.595	0.595	0.589	
R	1.2	0.548	0.574	0.529	0.550	

Table 5: Filling efficiencies for PPy(DBS) (Samples S through AA)

Sample	Charge Density (C/cm^2)	Filling Efficiency (Reduction 1)	Filling Efficiency (Reduction 2)	Filling Efficiency (Reduction 3)	Filling Efficiency (Average Per Sample)	Filling Efficiency (Average Per Charge Density)
S	0.4	0.662	0.668	0.662	0.664	0.712
T	0.4	0.795	0.808	0.738	0.780	
U	0.4	0.644	0.716	0.715	0.692	
V	0.8	0.610	0.626	0.620	0.619	0.638
W	0.8	0.541	0.564	0.575	0.560	
X	0.8	0.744	0.732	0.730	0.735	
Y	1.2	0.519	0.483	0.439	0.480	0.576
Z	1.2	0.478	0.748	0.763	0.663	
AA	1.2	0.582	0.589	0.587	0.586	

Filling efficiencies per charge density are approximately equal across all dopants. Due to the similar morphology shared by the dopants, the number of redox sites present in each membrane is roughly equivalent. As can be seen from Equation 3, if charge deposited during polymerization is held constant, then filling efficiency becomes a function of the number of available redox sites.

As charge density increases, the mass of PPy formed also increases, which in turn increases membrane thickness. Ions favor ingression to redox sites near the polymer surface. While the relationship between filling efficiency and charge density is not strictly linear as shown in [16], filling efficiency tends to decrease as charge density increases. At higher charge densities, membrane thickness impedes ingression and decreases filling efficiency.

Chapter 4: Conclusion

4.1 Contributions

Developing countries experience not only a disproportionate burden of disease for infectious diseases but also share rates of non-communicable disease equivalent to that of their developed counterparts. If fully realized, LOCs offer a means of providing affordable, accessible, and rapid diagnosis of a multitude of conditions to even the most remote places on Earth. Unfortunately, LOC design is currently hindered by its reliance on microfluidics. CPs, such as PPy, offer a novel alternative to the use of microfluidics in LOCs that could significantly simplify future design.

The purpose of this research was to determine the impact small changes in dopant morphology had on the properties of PPy. The experiments conducted through this research further develop scientific understanding of PPy and its potential use as a chemical actuator in LOCs. Multiple parameters characterizing the behavior of PPy(PTS), PPy(DS), and PPy(DBS) were explored:

- Ion transport was observed from the CVs to be reversible in PPy(DBS) and PPy(DS) but irreversible in PPy(PTS).
- Of the three polymers, PPy(DBS) had the sharpest redox peaks. Diffusion of ions near the peaks occurs more rapidly in PPy(DBS). PPy(DBS) also had the most positive reduction peak potentials, indicating the greatest affinity for storage of K^+.
- As charge density increases, the number of ions removed from solution increases. Higher charge densities equate to thicker membranes and the presence of more redox sites.

- From the pole-residue analysis, a linear relationship between residue and charge density was established.
- Filling efficiency was approximately equal across PPy variants at each charge density. At each charge density, the polymers possessed a similar number of redox sites due to the common morphology shared by their dopants.

Therefore, using the findings presented in this study, custom PPy membranes could be fabricated to match design specifications (such as those for LOCs) by varying dopant and charge density without sacrificing filling efficiency.

4.2 Recommendations for Future Work

Although the motivation behind this project is the development of novel healthcare devices, no experiments were conducted in cellular environments. Studying how these polymers perform in such environments would be a necessary step before a functional LOC could be designed, let alone viable for use on human patients.

A less complex recommendation would be refinement of the code that applies the second-order exponential fit to reduction cycles. While the fit does accurately model the transport processes, it is highly sensitive to the beginning and end points selected. A more robust code would reduce uncertainty.

Another possible area of expansion would be the design of a chamber that would hold all the electrodes in place during experiments. For this project, electrodes were suspended in solution using micromanipulators, and the distance between electrodes varied between samples. A chamber that maintained fixed electrode distances would improve the consistency of sample testing and hopefully decrease the variance observed in the Pole 1 values.

References

[1] World Health Organization, “2016 world malaria report”, WHO, Geneva, Switzerland, ISBN 978-92-4-151171-1, 2016

[2] C. Chin *et. al.*, “Lab-on-a-chip devices for global health: Past studies and future opportunities”, *Lab Chip*, vol. 7, pp. 41 – 57, 2006

[3] H. Wang *et. al.*, “Global, regional, and national life expectancy, all-cause mortality, and cause-specific mortality for 249 causes of death, 1980–2015: a systematic analysis for the Global Burden of Disease Study 2015”, *Lancet*, vol. 388, no. 10053, pp. 1459 – 1544, 2016

[4] A. Daar *et. al.*, “Top ten biotechnologies for improving health in developing countries”, *Nat. Genet.*, vol. 32, pp. 229 – 232, 2002

[5] D. Figeys *et. al.*, “Lab-on-a-chip: A revolution in biological and medical sciences”, *Anal. Chem.*, vol. 72, pp. 9, 330A – 335A, 2000

[6] A. Foudeh *et. al.*, “Microfluidic designs and techniques using lab-on-a-chip devices for pathogen detection for point-of-care diagnostics”, *Lab Chip*, vol. 12, pp. 3249 – 3266, 2012

[7] S. Sharma *et. al.*, “Point-of-care diagnostics in low resource settings: Present status and future role of microfluidics”, *Biosensors*, vol. 5, pp. 577 – 601, 2015

[8] D. Beebe *et. al.*, “Physics and applications of microfluidics in biology”, *Annu. Rev. Biomed. Eng.*, vol. 4, pp. 261-286, 2002

[9] D. Mark *et. al.*, “Microfluidic lab-on-a-chip platforms: requirements, characteristics and applications”, *Chem. Soc. Rev.*, vol. 39, pp. 1153-1182, 2010

[10] R. Ansari, “Polypyrrole conducting electroactive polymers: Synthesis and stability studies”, *E-J Chem.*, vol. 3, no. 4, pp. 186 – 201, 2006

[11] D. Ateh *et. al.*, “Polypyrrole-based conducting polymers and interactions with biological tissues”, *J. R. Soc. Interface*, vol. 3, pp. 741 – 752, 2006

[12] A. Ramanaviciene *et. al.*, “Biocompatibility of polypyrrole particles: An in-vivo study in mice”, *J. Pharm. Pharm. Sci.*, vol. 59, pp. 311 – 315, 2007

[13] D. Gallego-Perez *et. al.*, “Topical tissue nano-transfection mediates non-viral stroma reprogramming and rescue”, *Nat. Nanotechnol.*, vol. 12, no. 10, pp. 1 – 6, 2017

[14] M. De Paoli *et al*., “Properties of electrochemically synthesized polymer electrodes—x. study of polypyrrole/dodecylbenzene sulfonate”, *Electrochim. Acta*, vol. 37, no. 7, pp 1173 – 1182, 1992

[15] V. Venugopal and V.B. Sundaresan, “Polypyrrole-based amperometric cation sensor with tunable sensitivity”, *J. Intel. Mat. Syst.Str.*, vol. 27, no. 12, pp. 1702 – 1709, 2016

[16] R. Northcutt and V.B. Sundaresan, “Mechanoelectrochemistry of PPy(DBS) from correlated characterization of electrochemical response and extensional strain”, *Phys. Chem. Chem. Phys.*, vol. 17, no. 48, pp. 32268 – 32275, 2015

[17] L. Warren *et. al.*, “A study of conducting polymer morphology the effect of dopant anions upon order”, *J. Electrochem. Soc.*, vol. 136, no. 8, pp. 2286 – 2294, 1989

[18] T. Raudsepp *et. al.*, “Study of the factors determining the mobility of ions in the polypyrrole films doped with aromatic sulfonate anions”, *Electrochim. Acta*, vol. 53, pp. 3828-3835, 2008